Circularization, Photomechanical Switching, and a Supercoiling Transition of Actin Filaments

T. Sanchez,[1] I. M. Kulic,[2] and Z. Dogic[1]

[1]*Department of Physics, Brandeis University, Waltham, Massachusetts 02454, USA*
[2]*CNRS, Institut Charles Sadron, 23 rue du Loess BP 84047, 67034 Strasbourg, France*

(Received 30 July 2009; published 5 March 2010)

We confine actin filaments onto a 2D surface using depletion interactions and show that this significantly increases the probability of intramolecular circularization. Quantitative analysis reveals that the resulting semiflexible rings fluctuate significantly less then their linear counterparts with equal stiffness—an effect induced by the constraint of circular geometry. When exposed to fluorescence excitation light, rhodamine-phalloidin-labeled filaments undergo a change in their natural twist. This photomechanical transition induces a localized small-wavelength supercoiling transition of absorbed actin rings. Upon completion of the photoinduced reaction, the twist of neighboring monomers in an actin filament changes by approximately 0.26°.

DOI: 10.1103/PhysRevLett.104.098103 PACS numbers: 87.16.Ka, 82.35.Pq, 87.15.−v

A conceptually simple procedure of joining the two ends of a linear filament in order to form ring polymers has dramatic consequences, both on the conformations and fluctuations of single polymers as well as on properties of its bulk suspensions [1]. One important difference between multistranded linear polymers and their circularized counterparts is that the former easily relieve twist while the latter do not. As a consequence, circular polymers can undergo a supercoiling transition, a process that can be described using classical methods of statistical mechanics [2,3]. These theoretical developments have a direct application to the biological realm, where the circular form of DNA is essential for replication and survival of many different forms of life [4]. Because of its importance, cells contain a myriad of accessory proteins which regulate the circular and supercoiled state of the DNA [5]. In contrast to DNA, most other biopolymers assemble only into linear filaments. Filamentous actin (F-actin) is composed of globular subunits (G-actin), which spontaneously polymerize with increasing ionic strength. The basic structure of an actin filament is a right-handed helix, 8 nm in diameter, which repeats every 13 subunits [6]. In this Letter we describe a simple physical method for converting linear actin filaments into ring polymers.

When complementary ends of two actin filaments approach each other they can spontaneously anneal to produce longer linear polymers [7]. In principle, the two ends of the same actin filament could also join together to form ringlike structures. However, in solution this is an exceedingly rare event and formation of actin rings has not been reported so far. To circumvent this problem, we confine actin filaments onto a 2D surface and show that this significantly enhances the probability of intramolecular end-to-end annealing. We characterize in detail the fluctuations of the resulting filament rings. Surprisingly, we find that upon illumination, actin rings undergo a supercoiling transition due to a change in their twist. The importance of our studies stems from the fact that both DNA and actin are described with the same coarse-grained semiflexible rod model. This universality makes actin a particularly useful system for studying the dynamics of semiflexible biopolymers in general and rings and their supercoiling transition in particular. Because of its large persistence length (17 μm) [8], it is possible to directly visualize the instantaneous conformation of actin filaments, while the same is more difficult for DNA. Note that toroidal actin bundles (DNA toroid analogs) can be readily observed under various experimental conditions [9]. However, these cross-linked multifilament structures are very different from single filament rings described in this Letter.

Actin was purified from chicken skeletal muscle and labeled with either Alexa-488 phalloidin or rhodamine phalloidin [8]. Fluorescence intensity analysis reveals that in all our experiments more then 90% of the binding sites are occupied by phalloidin. All samples contained 200 mM KCl, 20 mM phosphate (pH = 7.5), 30% sucrose, and oxygen scavenging enzymes [8]. Cover glass and cover slips were cleaned in 0.5% detergent solution. Actin filaments were observed with epifluorescence microscope (Nikon TE2000) equipped with an electron multiplying charge coupled device (EMCCD) camera (Andor iXon 897) and 100 W mercury arc lamp. The intensity of the excitation light used to visualize rhodamine filaments is approximately 3 μW/μm^2. Quasi-2D suspensions of actin filaments are prepared by adding nonadsorbing polymer dextran (M.W. 500 000) to a final concentration of $c_{\mathrm{dex}} = 0.65\%$. This results in an effective attractive depletion potential between actin filaments and a surface, whose strength can be tuned by changing the polymer concentration [10]. We estimate that the effective adsorption energy density at dextran concentration at $c_{\mathrm{dex}} = 0.65\%$ is $\varepsilon_{\mathrm{ads}} = 0.5 k_B T/\mu$m [11]. We limit the number of adsorbed filaments to less then 10 per field of view (250 × 250 μm^2). This enhances the rate of intramolecular annealing which produces the desired ring structures and simultaneously suppresses in-

 © 2010 The American Physical Society

termolecular annealing which results in long linear filaments.

In free solution, actin circularization is a rare event. However, under quasi-2D confinement this effect is significantly enhanced. We find that, within a few hours of preparing a sample, approximately one in a few thousand filaments is found in a circular form. In the typical situation where the polymer's persistence length l_p, contour length L, diameter a, and the width of the quasi-2D confinement layer d satisfy the conditions $a < d \ll l_p \sim L$, a simple scaling estimate of the circularization rate enhancement gives $\omega_{2D}/\omega_{3D} \sim d^{-1}L^{3/2}l_p^{1/2}$ [12]. Here ω_{2D}/ω_{3D} denote the rates of circularization under quasi-2D confinement and in 3D (free solution). For typical values in our experiments ($L \sim l_p = 17$ μm and $d \approx 20$ nm the width of the depletion layer) the above estimate gives a circularization enhancement of $\omega_{2D}/\omega_{3D} \approx 10^3$, explaining the relatively frequent occurrence of actin rings under 2D confinement.

We first study the fluctuations of ring polymers. Their structure imposes strong constraints which are not present in linear filaments. To quantify this, we characterize a 2D filament by its in-plane tangent angle $\Phi(s)$, which is a function of arclength s. For $L \sim l_p$, $\Phi(s) = \frac{2\pi}{L}s + \phi(s)$, where $\frac{2\pi}{L}s$ represents the circular ground state and $\phi \ll 1$ is a small angular fluctuation around it. Apart from angular periodicity $\phi(0) = \phi(2\pi)$ the fluctuations also obey the ring closure constraint, $\int e^{i\Phi(s)}ds = 0$ (in x or y directions). After expansion in Fourier modes $\phi(s) = \sum \phi_n e^{2\pi i n s/L}$, the latter constraint implies $\phi_1 = 0$ to linear order. It follows that the correlation function and mean-squared tangent angle fluctuation are given by

$$\langle \phi(s)\phi(s')\rangle_{\text{ring}} = \frac{L}{2\pi^2 l_p}\sum_{n=2}^{\infty}\frac{1}{n^2}\cos\frac{2\pi n(s-s')}{L}, \quad (1)$$

$$\langle \phi^2\rangle_{\text{ring}} = \frac{1}{12}\left(1-\frac{6}{\pi^2}\right)\frac{L}{l_p}. \quad (2)$$

It is insightful to compare the latter result to the fluctuations of a linear filament with identical L and l_p about its ground state (straight configuration): $\langle \phi^2\rangle_{\text{lin}} = \frac{1}{6}\frac{L}{l_p}$. The reasons for the strong ≈ 5.1-fold reduction of fluctuations of ring polymers are the periodic boundary conditions and the circular closure constraints, as has been noted previously [2]. Experimentally, we measure $\langle \phi^2\rangle$ for both linear and ring polymers as a function of their contour length [Fig. 1(b)], finding linear dependence of $\langle \phi^2\rangle$ on L as predicted by theory. Experiments also confirm that the fluctuations of ring polymers are suppressed fivefold when compared to linear filaments. The fits of experimental data yield an independent measurement of actin's persistence length of 21.1 ± 2.2 μm for the rings and 22.0 ± 2.65 for the filaments. Both measurements fall within the confidence interval of the previously reported value of 17 ± 2.8 μm [8]. In addition to tangential fluctuations we also analyze the anisotropy of ring structure in Fig. 1(c). For small L/l_p the average ring conformation is close to a circle, i.e., there is very little anisotropy; with increasing ring size the average conformation becomes increasingly anisotropic. The mean shape anisotropy parameter Σ is measured by taking the ratio of the means of the smaller to larger eigenvectors of the moment of inertia tensor: $\Sigma = \langle R^2_{\text{min}}\rangle/\langle R^2_{\text{max}}\rangle$. Theory predicts that $1 - \Sigma \propto L^{(1/2)}$, which falls well within the confidence interval of our measured scaling exponent of $0.41 \pm .15$ [13].

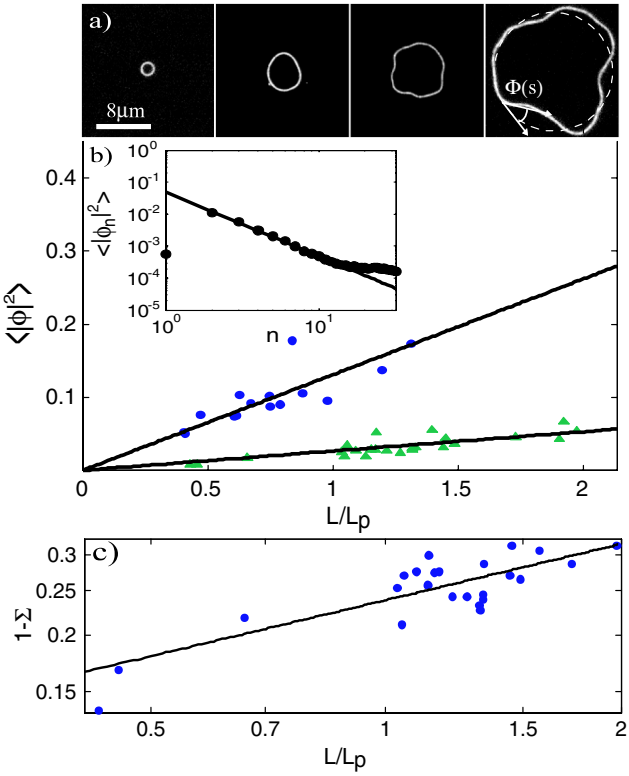

FIG. 1 (color online). (a) Images of fluorescently labeled actin rings. (b) Linear plot of the mean angular fluctuation of rings (solid triangles) and linear polymers (circles) as a function of contour length. Straight lines are theoretical predictions. Inset: Log-log plot of the fluctuation spectrum of a circular filament as a function of mode number. The fluctuations of the first mode are suppressed by the circularity constraint. Solid line indicates the spectrum of a linear filament with $l_p = 17$ μm. (c) Log-log plot of the mean anisotropy of the rings ($1 - \Sigma$) as a function of contour length. The anisotropy scales as $L^{0.41\pm0.15}$.

In contrast to linear filaments which easily relieve any excess twist, accumulation of twist in circular polymers can induce a transition to a supercoiled state. Surprisingly, we find that illuminating actin rings induces such a transition [Fig. 2(a)]. From simple observations of this process we draw a number of conclusions about the nature of the supercoiling transition. First, since it involves local desorption of filaments from the surface, the supercoiling transition is sensitive to dextran concentration c_{dex}, which determines the adhesion strength. We only observe supercoiling transition for $0.5\% < c_{\text{dex}} < 0.8\%$. For $c_{\text{dex}} <$ 0.5% filaments do not adsorb onto the surface, while for

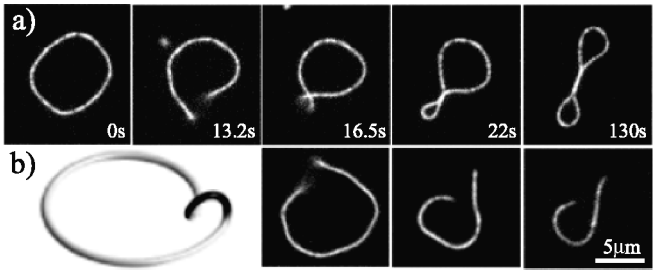

FIG. 2. (a) Images of an actin ring as it undergoes a photo-induced supercoiling transition. (b) Conformation of three different actin rings taken at the initial stage of the supercoiling transition. The right-handed outward spiral pattern is observed in all rings at the point of transition, identifying a consistent chirality. The 2D geometry implies a left-handed supercoil illustrated in the schematic.

$c_{\mathrm{dex}} > 0.8\%$ strong filament-surface attraction suppresses supercoiling on experimental time scales. Second, the supercoiling transition occurs only after the filaments have been illuminated with fluorescent excitation light. Furthermore, the supercoiling transition is sensitive to the nature of the fluorophore. Although both Alexa-488 and rhodamine-phalloidin actin rings have been studied, only the latter ones undergo a supercoiling transition. Finally, analysis of actin rings, as the supercoiling event takes place, reveals that the portion of the filament remaining adsorbed onto the surface always assumes a right-handed outward spiral pattern [Fig. 2(b)], implying that the transition induces a left-handed supercoil. Since actin is a right-handed helix, it follows that the supercoiling is induced by an overtwisting transition.

The presence of the depletion force changes the nature of the supercoiling transition. A ring supercoiling in free solution is known to become unstable at the longest geometrically available mode [14]. In contrast, the initial supercoiling transition for rings under quasi-2D confinement occurs at short length scales compared to the ring lengths. This small-scale supercoiling results from the interplay of the ring's bending energy, twisting energy, and the surface adsorption energy. Modeling this theoretically, we can extract a quantitative estimate for the energy barrier ΔE, as well as the excess linking number density σ, induced in the filament at the transition point. For a small out-of-plane ring fluctuation $z \ll L$, Fuller's formula [15] for $\phi \ll 1$ implies the ring writhe $\mathrm{Wr} = -(2\pi)^{-1} \times \int \phi' z' ds$. We can now apply the Calugareanu conservation theorem $\mathrm{Lk} = \mathrm{Tw} + \mathrm{Wr}$ [15], where Lk is the linking number and Tw is the twist. For $z/L \ll 1$, $\sigma L \gg 1$, the total energy reads $E \approx \int \{\frac{1}{2} B[\phi'^2 + z'^2 - (2\pi/L)^2 z'^2] + 2\pi\sigma C\phi' z' ds + V(z)\} ds$, with $B \approx 7 \times 10^{-26}\ \mathrm{N\,m^2}$ the bending stiffness, $C \approx B$ the torsional stiffness [16], and V the effective surface adsorption energy density. This term is modeled as a step function $V(z) = -\varepsilon_{\mathrm{ads}}$ for $z < d \ll L$ and 0 otherwise, with a constant adsorption line density $\varepsilon_{\mathrm{ads}}$. To understand the supercoiling kinetics via the activated formation of small loops with length $l \ll L$ we can subdivide the ring in a long adsorbed segment of length $L - l$ and a short desorbed loop segment of length l. Approximating the out-of-plane loop segment by a slender helix of arclength length l and radius $r \ll l$ (cf. Figure 2) and neglecting the small bending energy variation of the weakly curved in-plane ring part (and irrelevant constants), we obtain the energy

$$E = 2\pi^2 B\alpha^2 l^{-1} + 4\pi^2 C|\sigma|\sqrt{1-\alpha^2} + \varepsilon_{\mathrm{ads}} l, \quad (3)$$

with $\alpha = (2\pi r/l)^2$. This expression has a stable uncoiled state at $r = 0$ and a saddle barrier point (l_c, r_c)—the "critical loop state." For $r \ll l \ll L$ the transition state is at $l_c \approx (B/C)|\sigma|^{-1}$, $r_c \approx (2\sqrt{2}\pi^2)^{-1} \varepsilon_{\mathrm{ads}}^{1/2} B^{3/2} C^{-2} \sigma^{-2}$ with an energy barrier height $\Delta E \approx (B/C)|\sigma|^{-1}\varepsilon_{\mathrm{ads}}$. Short loops necessitate higher bending energy while longer ones require larger desorption energy, with an optimum in between. The ring remains flat ($r \approx 0$) until barrier crossing becomes kinetically accessible. As σ builds up over time the energy barrier decreases and the critical radius of the desorbed loop $2r_c$ shrinks. Eventually, thermal fluctuations push the filament over the barrier. From experimental measurements we determine the total length of the desorbed portion of the filament to be $l_c = 5.2 \pm 1.8\ \mu\mathrm{m}$ (16 measurements) and that it is independent of ring circumference; cf. Fig. 2. Using this with $\varepsilon_{\mathrm{ads}} = 0.5 k_B T/\mu\mathrm{m}$ we estimate a critical loop radius $r_c \approx 150$ nm and $\sigma_c = 0.2\ \mu\mathrm{m}^{-1}$ at the transition point. The energy barrier, estimated to be $\Delta E \approx 2.5 k_B T$, is small enough that thermal effects can induce a transition to supercoiled state. At higher depletant concentrations (larger ΔE) we do not experimentally observe a supercoiling transition in agreement with theoretical predictions.

The existence of an energy barrier precludes a quantitative analysis of twist accumulation from images such as those shown in Fig. 2. To quantify the switching transition kinetics we directly measure the rotation of actin filaments by holding the filament between two optically trapped beads and monitoring the rotation of the beads (Fig. 3). From these experiments we draw several conclusions. First, the excess twist accumulates gradually over a period of minutes. Thus the switching between the two states is not highly cooperative. Rather, monomers switch individually into overtwisted state upon photon adsorption. Second, the trapped beads rotate consistently in a right-handed fashion which implies that the accumulated twist is right handed, in agreement with conclusions drawn from Fig. 2(a). Third, increasing excitation intensity increases the velocity of bead rotation. Fourth, the bead angle as a function of time [Fig. 3(b)] can be described by an exponential function $\Psi(t) = \Psi_0(1 - e^{-t/t_{\mathrm{rel}}})$ where $t_{\mathrm{rel}} = 67s \pm 13.5$ (four measurements) is the characteristic time of the photoconversion. From here we determine the excess linking number $\sigma_{\mathrm{max}} = \Psi_0/(2\pi L) = 0.26\ \mu\mathrm{m}^{-1}$ and an angular change of $0.26° \pm 0.1°$ per monomer (eight measurements). These results are consistent with previous

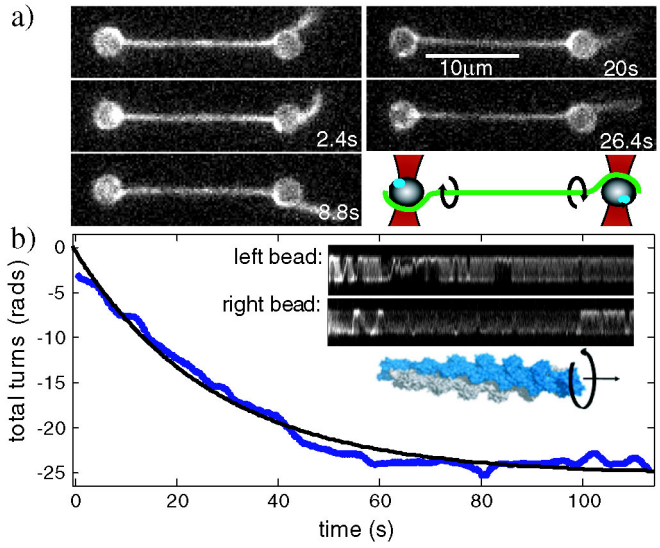

FIG. 3 (color online). (a) Twisting of an actin filament held in place with two optical traps. Schematic of the experimental setup: Biotin labeled filaments are attached to 2 μm streptavidin coated polystyrene beads which are simultaneously labeled with small 40 nm fluorescent biotin-tagged bead. Schematics of the setup is shown in bottom right. (b) The angular bead position of fluorescent 40 nm beads after exposure to fluorescence excitation light. The data are described by an exponential. Inset: Kymographs of the y position of the 40 nm fluorescent beads which indicate the rotation of large beads.

estimates of the excess linking number obtained from the analysis of adsorbed filaments (Fig. 2). Finally, the characteristic photoconversion time is comparable to the fluorescence bleaching time, $\tau = 80.4$ s.

In conclusion, we describe a novel method for self-assembly of ring polymers and report the first circularization of actin. We observe that semiflexible rings display strongly reduced tangent fluctuations compared to their linear counterparts—an effect caused by the circularity constraint. Most importantly, we report a novel light driven conformational transition of actin leading to ring supercoiling. Under partial 2D confinement, supercoiling becomes an activated process on small scales as opposed to the classical Mitchell instability [14]. Using two independent methods, we determine that the underlying polymorphic actin transition is right handed and that actin overtwists by 0.26° per monomer. Our experiments also have implications for biology where polymorphic transitions of actin filaments have recently received increased attention [17]. For example, in Limulus sperm, overtwisting of actin drives a fast mechanical transition of an actin bundle. Interestingly, the change in monomer twist between the extended and coiled states of Limulus sperm actin bundle is 0.23° [18], a value very similar to our findings. Thus, our experiments raise the possibility of designing photoinduced biomimetic nanostructures, capable of converting structural transitions of actin filaments into mechanical work and open a path towards well-controlled photoactuation of contractile actin bundles, networks, and gels. Finally, we also note that rhodamine phalloidin is frequently used for directly visualizing various actin structures. Our experiments indicate that great care is needed when interpreting these experiments, due to the existence of photoinduced changes in the actin structure.

This work was supported by NSF through Grants No. DMR-0705855 and No. DMR-MRSEC-0820492. I. M. K. thanks A. Johner and H. Mohrbach for support and fruitful discussions.

[1] M. Kapnistos *et al.*, Nature Mater. **7**, 997 (2008); R. M. Robertson and D. E. Smith, Proc. Natl. Acad. Sci. U.S.A. **104**, 4824 (2007).
[2] K. Alim and E. Frey, Phys. Rev. Lett. **99**, 198102 (2007); Eur. Phys. J. E **24**, 185 (2007).
[3] C. J. Benham, Biopolymers **22**, 2477 (1983); Proc. Natl. Acad. Sci. U.S.A. **74**, 2397 (1977).
[4] A. D. Bates and A. Maxwell, *DNA Topology* (Oxford University Press, New York, 2005).
[5] R. Philips, J. Kondev, and J. Theriot, *Physical Biology of the Cell* (Garland Science, New York, 2009).
[6] E. H. Egelman, N. Francis, and D. J. DeRosier, Nature (London) **298**, 131 (1982).
[7] D. Popp, A. Yamamoto, and Y. Maeda, J. Mol. Biol. **368**, 365 (2007).
[8] C. P. Brangwynne *et al.*, Biophys. J. **93**, 346 (2007).
[9] J. X. Tang *et al.*, Eur. Biophys. J. **30**, 477 (2001); A. W. C. Lau *et al.*, Europhys. Lett. **87**, 48 006 (2009); L. Limozin and E. Sackmann, Phys. Rev. Lett. **89**, 168103 (2002); M. M. A. E. Claessens *et al.*, Nature Mater. **5**, 748 (2006); A. Kadota and M. Wada, Protoplasma **151**, 171 (1989).
[10] S. Asakura and F. Oosawa, J. Chem. Phys. **22**, 1255 (1954).
[11] T. Sanchez *et al.* (to be published).
[12] The circularization rate is assumed to be proportional to the probability of two ends being within a short "capture" distance a. For short chains $L \sim l_P$ this probability p can be decomposed into an in-plane $p_\parallel$ and out-of-plane contribution $p_\perp$. $p_\perp(d)$ indicates our out-of-plane contribution with d the thickness of confinement layer. For $a < d \ll L$, $p_\perp(d) \sim a/d$, while for $d \gg L$, $p_\perp(\infty) \sim a/\Delta z$, with $\Delta z \sim L^{3/2} l_p^{-1/2}$. Thus $\omega_{2D}/\omega_{3D} \sim p_\perp(d)/p_\perp(\infty) \sim L^{3/2} d^{-1} l_p^{-1/2}$.
[13] C. J. Camacho *et al.*, J. Chem. Phys. **94**, 5693 (1991).
[14] J. H. Michell, Messenger Math. **11**, 181 (1889); A. Goriely, J. Elast. **84**, 281 (2006).
[15] F. B. Fuller, Proc. Natl. Acad. Sci. U.S.A. **68**, 815 (1971).
[16] Y. Tsuda *et al.*, Proc. Natl. Acad. Sci. U.S.A. **93**, 12 937 (1996).
[17] E. H. Egelman, Nat. Rev. Mol. Cell Biol. **4**, 621 (2003); J. Kozuka *et al.*, Nature Chem. Biol. **2**, 83 (2006).
[18] D. DeRosier, L. Tilney, and P. Flicker, J. Mol. Biol. **137**, 375 (1980); M. F. Schmid *et al.*, Nature (London) **104**, 431 (2004); L. Mahadevan and P. Matsudaira, Science **288**, 95 (2000).